Journal of Non-Crystalline Solids 600 (2023) 121989

Contents lists available at ScienceDirect

Journal of Non-Crystalline Solids

journal homepage: www.elsevier.com/locate/jnoncrysol

Revealing the structure of the sodium-leached layer of soda lime silica glass: A comprehensive spectroscopic analysis

Andrew L. Ogrinc [a], Yuxing Zhou [b], Seung Ho Hahn [c,†], Yen-Ting Lin [a], Seong H. Kim [a,*]

[a] Department of Chemical Engineering and Materials Research Institute, The Pennsylvania State University, University Park, PA 16802, USA
[b] Department of Materials Science and Engineering, University of Illinois, 1304 West Green Street, Urbana, IL 61801-3028, USA
[c] Department of Mechanical Engineering, The Pennsylvania State University, University Park, PA 16802, USA

ARTICLE INFO

Keywords:
IR spectroscopy
Glass
Molecular dynamics
Soda lime silica
Corrosion

ABSTRACT

Acid treatment of soda lime silica glass results in incongruent leaching of sodium from the surface, with minimal dissolution of the silicate network or the other cationic network modifiers. The structure of this sodium-leached region was probed using nanoscale-FTIR and Raman spectroscopy. After accounting for interfacial interference, the resultant spectra were compared with molecular dynamics simulations to connect the observed spectral changes to the structure. This comparison showed that the correlations between spectral features and bond parameter distributions derived from the melt-quench formed glass can also be applied to a chemically-modified glass. Additionally, the IR active shoulder at ~950 cm^{-1} which was traditionally attributed to the non-bridging oxygen stretch mode, was confidently correlated to perturbations in the silicate network which results from the network modifiers which charge compensate those non-bridging oxygen. The decrease in this spectral feature after acid treatment then corresponds to localized structural relaxations as the glass network becomes more silica-like.

1. Introduction

The surface properties of soda lime silica (SLS) glass have a large impact on the crack resistance, corrosion behavior, and tribological wear resistance. [1–3] Thus, understanding the surface and subsurface structures of SLS is very important. When a low aluminum glass such as SLS is exposed to an acidic solution, the mobile sodium cations in the surface region are leached from the glass network, as the glass undergoes a sodium-hydrogen (Na-H) ion-exchange process. [4–9] This ion-exchange process (also called Na-leaching) occurs with negligible silicate network dissolution. [10–15] Regardless of the exact mechanism, elemental depth profiling via x-ray photoelectron spectroscopy (XPS) and time-of-flight secondary ion mass spectrometry (TOF-SIMS) has consistently shown that sodium is depleted from about 150 nm of the surface after 1 week of treatment at 90 °C, while the depletion of calcium, magnesium, and aluminum are negligible. [2,5,10,11] Although elemental concentration profiles have been well resolved, the actual structure of the silicate network of this Na-leached layer is not well understood.

Vibrational spectroscopy such as specular reflection infrared spectroscopy (SR-IR) has been used to probe the structure of the surface layer. Previous studies have shown that after acid leaching, there is a shift in the strong peak near 1050 cm^{-1} to higher wavenumbers, and an enhancement in the shoulder centered around 950 cm^{-1}. [4–8] These two features have typically been attributed to the asymmetric stretching vibrational modes of the bridging oxygen (BO) of the silicate network, and the stretching vibrational mode of the non-bridging oxygen (NBO) associated with modifier ions in the network, respectively. [7,16–18] It was previously speculated that the enhanced intensity at 950 cm^{-1} after acid treatment was the result of depolymerization of the silicate network, as the intensity of this shoulder is generally correlated directly to the concentration of NBOs. [5,17] However, this analysis disregards the impact of the probe depth of SR-IR on the spectra. Based on the refractive index of the sample material, SR-IR is predicted to have a probe depth of around 1 μm in the Si—O stretch mode region, which is significantly larger than the Na-leached depth as determined via XPS depth profiling. [10,16] The secondary reflection off the leached layer/bulk interface will result in interference with the primary reflection off the glass surface, which will obscure the spectral details of the surface layer. [19] When not properly compensated for, these interfacial

* Corresponding author.
E-mail address: shk10@psu.edu (S.H. Kim).
† Current address: Mechatronics Research, Samsung Electronics Co. Ltd., Hwaseong 18448, South Korea.

https://doi.org/10.1016/j.jnoncrysol.2022.121989
Received 30 June 2022; Received in revised form 18 October 2022; Accepted 19 October 2022
Available online 2 November 2022

interference effects are enough to call all previously performed analysis into question.

This interfacial interference can be modeled when accurate values of the refractive index of the surface layer and bulk material are known. [20] Previously, Geotti-Bianchini et al. attempted to model the surface layer as identical to vitreous silica. [7] For ease of comparison, this data has been replotted in the Supporting Information (SI) section. Choosing vitreous silica could be justified because the Na-leached SLS layer is silica-rich in composition. [10] Despite this, the model had generally poor agreement with the experimental SR-IR result, failing to accurately model either the shift of the peak centered at 1050 cm^{-1} or the enhanced shoulder at 950 cm^{-1}. After further consideration, it makes sense that the Na-leached surface layer would be poorly modeled as identical to vitreous silica. In addition to containing a significant concentration of other elements (Ca, Mg, and Al), the Na-leached SLS will have a different thermal history than vitreous silica. This means that even if they were compositionally identical, their density, and therefore refractive indices and resultant spectra, could still be different. [12]

In this study, more accurate and realistic refractive index information for the Na-leached layer of SLS was attained via nanoscale-Fourier transformation infrared (nano-FTIR) spectroscopy measured via scattering-type scanning near field optical microscopy (sSNOM). Nano-FTIR is capable of measuring the dielectric constant of a material with a probe depth on the same length scale as the diameter of the nanoscale probe used for the measurement. [21] Using a metal-coated atomic force microscopy (AFM) tip, a probe depth between 20 and 100 nm can be achieved, which is well below the Na-leached layer depth measured by XPS depth profiling. [22,23] Dielectric constant values measured from nano-FTIR can be used to calculate the refractive index of the Na-leached SLS surface layer, which can then be compared with the Si—O bond length distributions obtained from molecular dynamics (MD) simulations. The validity of the MD simulations was also tested and confirmed by comparing the bending vibration modes in Raman spectroscopy with the Si—O—Si bond angle distributions. The good agreement between the nano-FTIR and Raman spectral features with the bond length and angle distributions of MD-simulated structures suggested that the silicate glass network undergoes significant structural relaxations upon the Na-H ion-exchange even through the leaching treatment is carried out about 500 °C below the glass transition temperature (T_g). This also clearly demonstrates that the 950 cm^{-1} shoulder of the pristine and Na-leached SLS glass network should not be interpreted as the stretch mode of Si-NBO bonds; it originates from the perturbation of the silicate network due to the presence of Na modifier ions which are associated with NBOs.

2. Experimental and simulation methods

2.1. Materials and sample preparation

Float glass sheets of SLS (0.7 mm thick) used in these experiments were provided by AGC (Tokyo, Japan). The provided glass panels were cut into 2.5 square cm pieces by scratching with a diamond tipped scribe, and were then bent to break at the scribed line. These pieces were thermally annealed at a heating rate of 8.33 C°/min over the course of 1 hour, then held at a temperature of 0.9 × T_g for 2 hours. The samples were then allowed to cool overnight in the furnace to room temperature. After thermal annealing, the samples were sonically cleaned in ACS grade acetone (VWR) and 100% ACS grade ethanol (Thermo Scientific).

The leaching solutions were prepared by mixing 150 mL of ASTM Type 1 DI Water (LabChem Inc) with 1 mL of 68 wt% nitric acid solution (Thermo Scientific) in a 250 mL perfluoroalkoxy (PFA) jar (Savillex Corporation) with a permeable Teflon sample basket, which was pre-heated to 90 °C overnight. The cleaned samples were then placed into the solution, resting on the sample basket to ensure equal expose of both sides of the slides to the acidic solution. After 7 days, the samples were removed from the solution, rinsed with excess ASTM Type 1 DI Water and blown with dry nitrogen. All of the analysis was performed on the air side of sample, to avoid any potential property changes that result from the tin contamination inherent to the Pilkington float process. [24, 25]

2.2. X-ray photoelectron spectroscopy

The depth of sodium leaching in the glass after 1 week of treatment was evaluated with X-Ray photoelectron spectroscopy (XPS) depth profiling. These analyses were conducted on a PHI VersaProbe III with a monochromatic Al-Kα X-ray source and a low-energy charge neutralizer. Accurate RSF values were determined by measuring the spectrum of the cross section of a sample that was fractured in-situ in the vacuum of the XPS chamber, then using the manufacturer's given composition to normalize the peak area. Elemental quantification was performed over narrow binding energy regions to measure the O1s, Na KLL, Ca2p, Mg KLL, C1s, Si2p, and Al2p peaks, averaging 3 scans at a pass energy of 117 eV. These peaks were chosen due to a similar inelastic mean free path of the ejected photoelectrons. [26] The binding energy of the peaks were calibrated by setting the advantageous carbon contamination peak to 284.6 eV.

Depth profiling was performed with an Ar^+ beam, with the profiling rate calibrated separately by determining the time needed to profile through a silicon wafer with a known oxide layer thickness. The analysis beam was focused to a 200 μm diameter circle in the center of the 2 mm by 2 mm profiling crater, to mitigate edge effects. To compensate for the migration of the sodium due to surface charging, the sodium to silicon ratio was normalized to the measured effective bulk value. This profile was then fit with an error function, with the depth where Na/Si = 0.5 corresponding to the true location of the interface. [27] This was also done to account for non-idealities inherent to quantification of the composition in a material via profiling. These non-idealities include preferential sputtering, surface roughness, and the probe depth of XPS. [28,29]

2.3. Spectroscopic analysis

SR-IR spectra of the pristine and Na-leached sample was collected with a Bruker Vertex V80 spectrometer with a Pike VeeMax II accessory, which allowed operation in specular reflection mode. The spectrum was collected in the mid-IR range (500 cm^{-1} to 4000 cm^{-1}) at an incidence angle of 30° under an inert nitrogen atmosphere to prevent interference from atmospheric water. The spectra were collected and averaged over 500 scans with a resolution of 5 cm^{-1}, and was referenced to a clean gold film. nano-FTIR spectroscopy measurements were collected with a neaSCOPE-IR+s scattering-type near-field optical microscope system from neaspec. For nano-FTIR spectroscopy, broadband mid-infrared supercontinuum laser pulses tunable in the spectral range between ca. 670-2100 cm^{-1} generated by a difference frequency generation laser source (FemtoFiber dichro mid-IR, Toptica) were focused onto a Pt/IR coated AFM tip (nano-FTIR tips, neaspec). The tip-scattered light was detected utilizing an asymmetric Michelson interferometer (nano-FTIR module, neaspec). Interferograms of the tip-scattered light were obtained by translation of the mirror in the reference arm and recording the detector signal as position of the reference mirror displacement. Subsequent Fourier transform of the interferograms yielded simultaneously near-field amplitude and phase spectra of the tip scattered fields.

The AFM of the s-SNOM setup was operated in intermittent contact mode, where the AFM tip was oscillated vertically (~50 nm) with a frequency (Ω) close to the mechanical resonance of the cantilever. For separating the near-field signal from spurious far-field signal contributions, demodulation of the detector signal at a higher harmonic (n) of W ($n \geq 2$) was used. Each sample spectrum was normalized to a reference spectrum measured on a clean silicon sample surface, yielding normalized near-field amplitude and phase spectra, $S_n/S_{n,(Si)}$ and ϕ_n-$\phi_{n,(Si)}$,

respectively. In this work, near-field amplitude and phase spectra with demodulation order n = 2 were used for analysis. All nano-FTIR spectra were recorded with a spectral resolution of 10 cm^{-1}. In order to improve the signal-to-noise of the nano-FTIR spectra, 25 individual nano-FTIR spectra acquired on the sample were co-averaged. Details of the calculation of the dielectric constant from S_2 and ϕ_2 can be found in the SI section.

Raman spectra of the pristine and acid treated samples was performed on a Horiba LabRAM HR Evolution confocal Raman microscope with a 100X objective lens (0.9 NA), equipped with a 364 nm laser to detect the Raman shift between 250 cm^{-1} to 3500 cm^{-1}. Based on the excitation wavelength and the NA of the objective lens, the depth of field was estimated to be 1.8 μm, which is taken as equivalent to the diffraction limit. [30,31] The spectrum of the Na-leached SLS was collected by first focusing the beam on the surface of the sample. The stage was then shifted vertically, and a depth profile in the z-direction was performed. [30] A spectra was recorded every few hundred nanometers, until the signal matched the spectra from the pristine sample. Then, the spectrum which was dominated by the Na-leached surface layer was selected for the analysis.

2.4. Molecular dynamics simulations

Atomic scale MD simulations were employed to simulate changes in the network structure after acid treatment. It would be ideal if one force field could simulate both bond parameter distributions and vibrational spectral features of the pristine and Na-leached SLS structures; but no such force field is available at this time. The 'rigid-ionic' Teter potential can simulate the structures of sodium silicate and sodium calcium silicate glasses, but its capability to predict vibrational spectrum is very poor. [32,33] Also, it is not properly parameterized to include hydrogen in the model. In contrast, the 'polarizable core-shell' FFSiOH potential can simulate the structure and vibrational spectral features of a glass consisting of Si, O and H; but it cannot handle other NMW ions. [33,34] ReaxFF, a reactive force field that employs bond-order concepts to empirically describe atomic interactions, can handle both alkali ions and hydrogen in the silicate glass network, but the simulated spectra do not adequately match experimentally collected spectra. [33,35,36] Additionally, the calcium description compatible with the Si—O—H—Na ReaxFF has not been fully developed for proper interpretation of sodium calcium silicate glasses. [36] As both the vibrational spectra and structure of the simulated glasses are of interest, the following strategy was used for the MD simulations. More specifics about the parameters used during simulation are provided after:

1 Initial glass structure generation
   1) A sodium silicate ($[Na_2O]_{0.166}[SiO_2]_{0.833}$ = $Na_{0.4}SiO_{2.2}$) and silica (SiO_2) structure were generated using the Teter potential to provide a common structural basis, as it is known to generate silicate glass structures more accurately than either ReaxFF or FFSiOH [32,33]
2 Simulation of the structural parameters
   1) The Teter-generated sodium silicate structure was relaxed with ReaxFF in NPT isobaric-isothermal conditions (1 atm, 300 K)
   2) Separately, the Na^+ ions in the Teter-generated sodium silicate structure were replaced with H^+, then the resulting $H_{0.4}SiO_{2.2}$ (referred to as "protonated silica" hereafter) was relaxed with ReaxFF in NPT isobaric-isothermal conditions (1 atm, 300 K)
   3) The Teter-generated silica was relaxed with ReaxFF in NPT isobaric-isothermal conditions (1 atm, 300 K)
   4) The structural parameters of the three structures were then extracted from the simulations
3 Simulation of the vibrational spectra
   1) The Na^+ ions in the Teter-generated sodium silicate structure were replaced with H^+, then the resulting protonated silica ($H_{0.4}SiO_{2.2}$) was relaxed with the FFSiOH force field
   2) The Teter-generated silica was also relaxed with the FFSiOH force field
   3) Vibrational spectra were extracted for both the simulated P-silica and silica glasses

Simulations with Teter and FFSiOH potentials were conducted with the GROMACS package following the protocol described previously. [37] The non-bonded three body interaction for H-bonding parametrized in FFSiOH was ignored in our simulation as it cannot be handled in GROMACS. We expect it has little effect on our results since it is suggested to be relevant only for strong H-bond interactions in the hydrogarnet defects, which is rare, if not absent, in our simulation. Simulations with ReaxFF were conducted with the LAMMPS package following the protocol described previously. [33]

3. Results and discussion

3.1. Deconvolution of the interfacial interference in SR-IR analysis of Na-leached SLS surface

Fig. 1A shows the XPS depth profile of an SLS sample treated in pH 1 at 90 °C. The XPS depth profiling confirms the existence of a sodium concentration gradient in the surface of the glass after acid leaching. The thickness of the Na-leached layer is found to be 131 ± 9 nm. Depth profiles with all elements shown can be found in the SI section. Fig. 1B compares the SR-IR spectra of pristine and Na-leached SLS surfaces. As described in Section 1, the apparent enhancement of the shoulder at 950 cm^{-1} is seen after acid leaching (marked with an orange background).

Fig. 1C displays the theoretical SR-IR spectra calculated using the refractive index values obtained from nano-FTIR analyses. Details of converting the near-field scattering signals from nano-FTIR to dielectric constants and then calculating the SR-IR spectrum from the obtained optical constants are shown in the SI section. It is noted that the SR-IR spectrum of the hypothetical glass with the Na-leached layer structure exhibits a clear decrease in intensity of the shoulder at 950 cm^{-1}, as compared to that of the pristine SLS glass. When the SR-IR spectrum of the 131 nm-thick Na-leached layer over pristine SLS is calculated using the refractive index of each component, then the 950 cm^{-1} shoulder region is enhanced, which is in good agreement with the experimental spectrum. This result clearly proves that the enhancement of the 950 cm^{-1} shoulder in experimental SR-IR analysis is the mere consequence of interference of the IR beams reflected from the air/leached layer interface and the leached layer/bulk glass interface.

Fig. 2 replots the theoretical SR-IR spectra, in absolute intensity scale, of pure silica, pristine SLS, and the hypothetical glass with the Na-leached layer structure, calculated using the refractive index obtained from nano-FTIR analysis of each type of glass. Unless a significant portion of NBO groups undergo condensation reactions during the leaching process, which would form Si—O—Si (BO) species (which is unlikely below 300 °C),[38] the total concentration of the NBO groups (either $Si—O^-$ or Si—OH) is expected to be conserved as the $Si—O^-$ groups will be converted stoichiometrically to the Si—OH groups. However, the Na-leached network has a decreased intensity of the shoulder at 950 cm^{-1} despite having the same concentration of NBOs as the pristine SLS. There must be a genuine reason for the decrease in the peak intensity at 950 cm^{-1} after acid treatment, despite a negligible change in the concentration of NBO units in the glass, which can be addressed using MD simulations.

3.2. Structural features of pristine and Na-leached SLS network from MD simulations

Fig. 3 compares the bond length and angle distributions of sodium silicate, protonated silica, and silica structures relaxed with ReaxFF. After the exchange, the Si—BO bond length distribution shifts to lower bond lengths by ~0.005 Å, towards the silica curve (Fig. 3A). It is

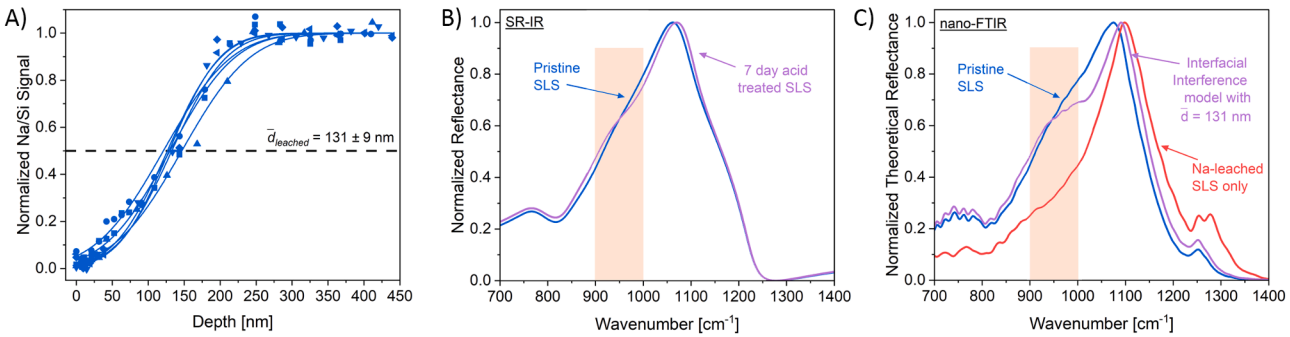

Fig. 1. (A) Depth profile of the Na/Si signal, determined with XPS and normalized to the effective bulk value, for SLS leached at pH 1 for 7 days at 90 °C. The measurements were repeated with six samples prepared separately to check the reproducibility of the leaching and depth profiling, which yielded good consistency. The leached depth was determined by fitting the concentration profile with the error function. (B) SR-IR spectra of pristine SLS and a sample with a sodium-leached surface layer from 7 days of acid treatment. The OH stretch region is shown in the SI section. (C) Theoretical reflectance as calculated using the refractive index measured in nano-FTIR for a pristine SLS sample, a Na-leached SLS sample (after 7 days of acid treatment), and one sample which models the interfacial interference using a 131 nm thick thin film of Na-leached SLS over bulk pristine SLS. Details of how sSNOM signals are converted to the refractive index in nano-FTIR, how theoretical SR-IR spectra are calculated from the refractive index, and more details of the interfacial interference model can be found in the SI section. Note that both experimental and theoretical SR-IR spectra are normalized for easy comparison of the relative intensities.

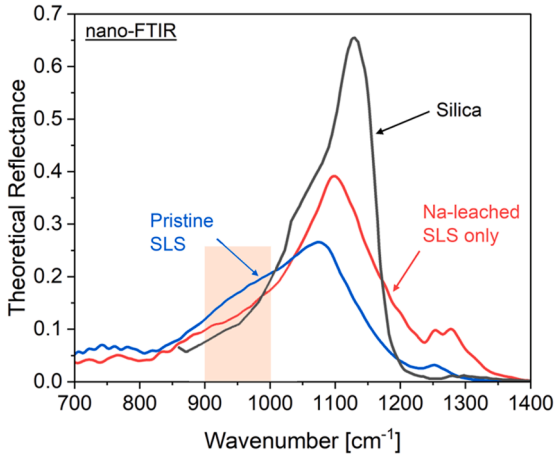

Fig. 2. Theoretical SR-IR spectra of silica, pristine SLS, and Na-leached SLS as simulated using the refractive index values measured from nano-FTIR. The silica spectrum is taken from He et al. [21].

intriguing to compare this value with the estimate from the experimental spectra. Based on the peak shift of the Si—O—Si stretch band towards a higher wavenumber after acid leaching in Fig. 2, and using the previously found empirical correlation between peak position and bond length distribution of silica and sodium silicate glasses, [33] the experimentally observed blue-shift of the peak position suggests that the average Si—O bond length distribution of the BO network is decreased by around 0.004 Å after acid treatment. This coincides well with the value found from MD simulations, shown in Fig. 3A. These results suggest that when the sodium ion associated with the NBO site is replaced with a proton, forming Si—OH in the glass network, the BO network is relaxed to a structure with a slightly shorter bond length distribution. Thus, it can be said that replacing sodium with hydrogen results in a glass network that is more silica-like. [4,5]

Fig. 3B shows that after the Na-H exchange, the Si—O—Si bond angle distribution shifts to higher values, towards the silica curve. While the change in the average O—Si—O bond angle distribution appears to be insignificant, a small decrease in the full-width-half-max (FWHM) (Fig. 3D) also seems to resemble the silica curve. To validate the Si—O—Si bond angle change shown in the ReaxFF simulations, the bending vibration mode in the Raman spectrum can be used. In previous studies, a negative correlation between the broad spectral feature below 650 cm^{-1} and the Si—O—Si bond angle distribution was found. [33,39]

Fig. 4A compares the Raman spectra of pristine and Na-leached SLS surfaces. It can be clearly seen that the lower wavenumber side of the bending vibration mode is enhanced after acid treatment (shown in the green area). This is in qualitative agreement with the trend seen in the comparison of sodium-silicate (which is the structure used to model SLS) and protonated silica (which is used as a model for the Na-H exchanged SLS) in Fig. 3B.

The SR-IR spectra simulated via the FFSiOH force field for silica and protonated silica shown in Fig. 4B are remarkably consistent with the SR-IR spectra calculated via nano-FTIR analysis of the silica and Na-leached SLS shown in Fig. 2. Despite the fact that the protonated silica has significantly more NBOs (Q^3 = 39.8% and Q^4 = 60.2%), the stoichiometric silica (SiO_2) and the protonated silica ($SiO_{2.2}H_{0.4}$) have a nearly identical intensity in the 950 cm^{-1} region. The presence of Si—OH groups with bond lengths slightly longer than the Si—BO bonds in the network length (Fig. 3C; also see the SI section for comparison of the Si—BO and Si—OH bond length distributions obtained with the FFSiOH force field) does not contribute to the spectral intensity at 950 cm^{-1}. They only give a broad band in the OH stretch region (2500 – 3800 cm^{-1}; the refractive index of the —OH stretch region as simulated in FFSiOH is shown in the SI section). In the spectra simulated with the FFSiOH force field, the protonated silica shows a lower Si—O stretch intensity at ~1100 cm^{-1} than the pristine silica (Fig. 4B). A similar trend is observed when the theoretical reflectance spectra of the silica and Na-leached SLS surfaces are compared (Fig. 2).

When considered as a whole, it seems that the acid treatment and subsequent Na-H ion-exchange is accompanied by significant structural changes in the glass structure. Nano-FTIR and ReaxFF both report that the average Si-BO bond length decreases by about 0.005 Å upon the Na-H exchange. Raman spectroscopy and ReaxFF both report an increase in the average Si—O—Si bond angle distribution. Nano-FTIR and FFSiOH both predict a decrease in the level of perturbation in the silicate network after acid treatment. These structural changes suggest localized structural relaxation in the glass network around the NBO ion-exchange sites (Fig. 5). In this context, the new interpretation of the 950 cm^{-1} spectral feature of the SLS glass (Fig. 2) is that it originates from perturbations in the glass network by the presence of cationic network modifiers (NWMs) which charge-compensate NBOs. As the Na is stoichiometrically replaced with H (forming Si—OH), the perturbations imposed by NWMs associated with NBOs to the surrounding BO network are relaxed or reduced (Fig. 3). These localized structural relaxations result in the Na-leached SLS becoming more silica-like, with a decreased Si—BO bond length, an increased Si—O—Si bond angle, and a narrower O—Si—O bond angle distribution. It is important to note that this silica-

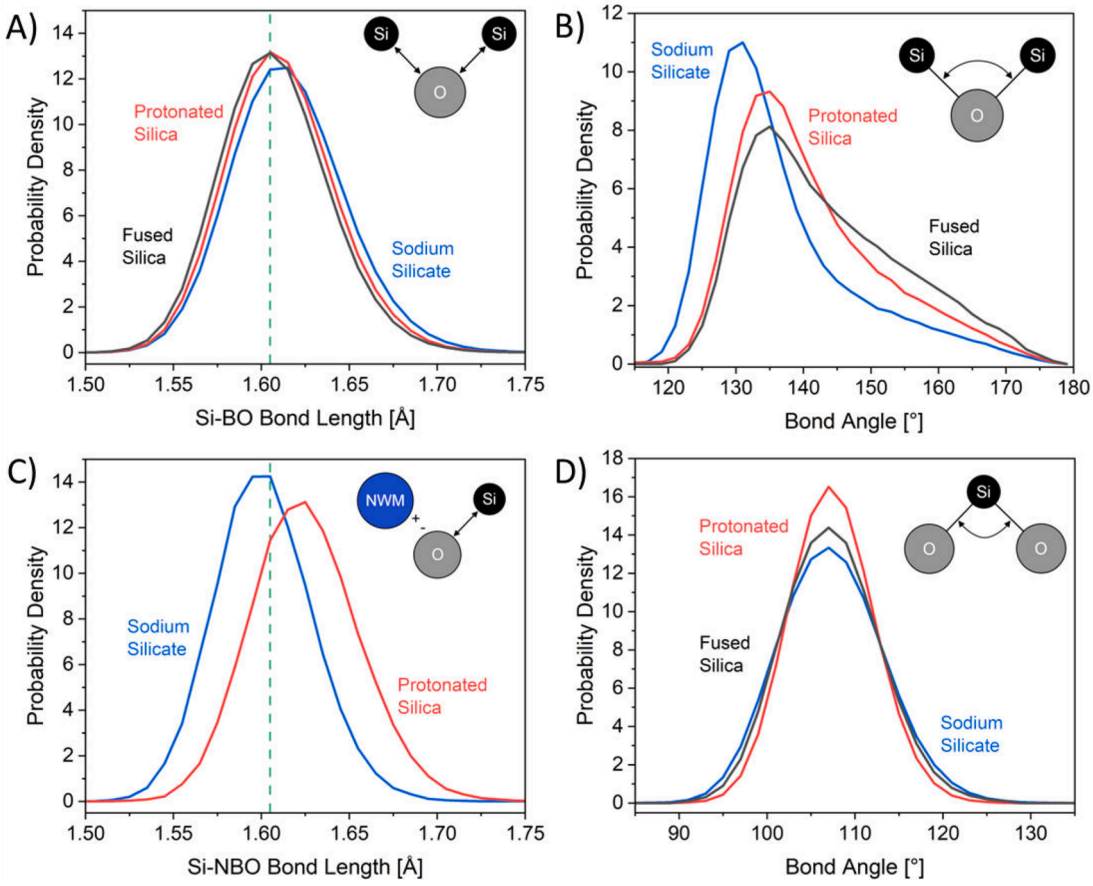

Fig. 3. (A) Si—BO bond length distributions, (B) Si—O—Si bond angle distributions, (C) Si—NBO bond length distributions, and (D) O—Si—O bond angle distributions for a sodium silicate (analogous to pristine SLS), protonated silica (analogous to the sodium-leached surface layer), and fused silica (pure glassy SiO_2) as simulated in ReaxFF. The sodium silicate and protonated silica have the same concentration of network modifiers, described by the formula (0.166) X_2O · (0.834) SiO_2. The distribution curve is area-normalized.

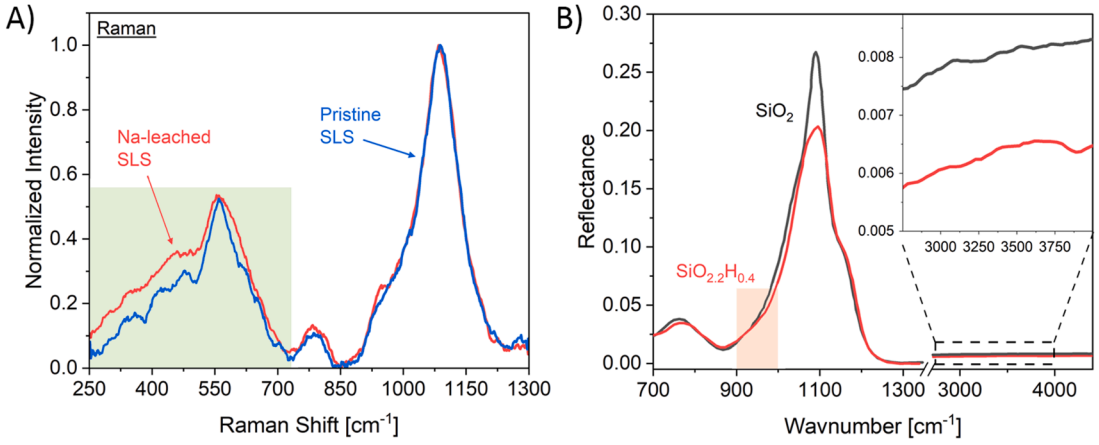

Fig. 4. (A) Raman data collected with a 364 nm laser for the acid treated SLS and pristine SLS, normalized to the maximum signal intensity. The raw data can be found in the SI section. (B) The simulated vibrational spectra for the simulated silica and protonated silica structures, with an inset showing the –OH stretch region from 2750 cm^{-1} to 4000 cm^{-1}. The optical constants of the silica and protonated silica are shown in the Supporting Information.

like structure is still distinct from the structure of fused silica, as they have different thermal histories. [12]

3.3. Origin of misconception for the 950 cm^{-1} shoulder in SR-IR

Here we review the historic origin for relating the observed enhancement at 950 cm^{-1} to the concentration of NBOs in the glass, which is the standard peak assignment in the field, and the reason why it is insufficient. [4,18,33,40,41] Sanders et al. observed that the shoulder at 950 cm^{-1} increased in proportion to the concentration of alkali modifier ions. [17] By assuming that SR-IR probed isolated vibrational modes (which was a wide-spread concept in the 1970s), a Beer-Lambert law type argument was applied to the normalized change in the spectral intensity, which resulted in a linear correlation between the 950 cm^{-1}

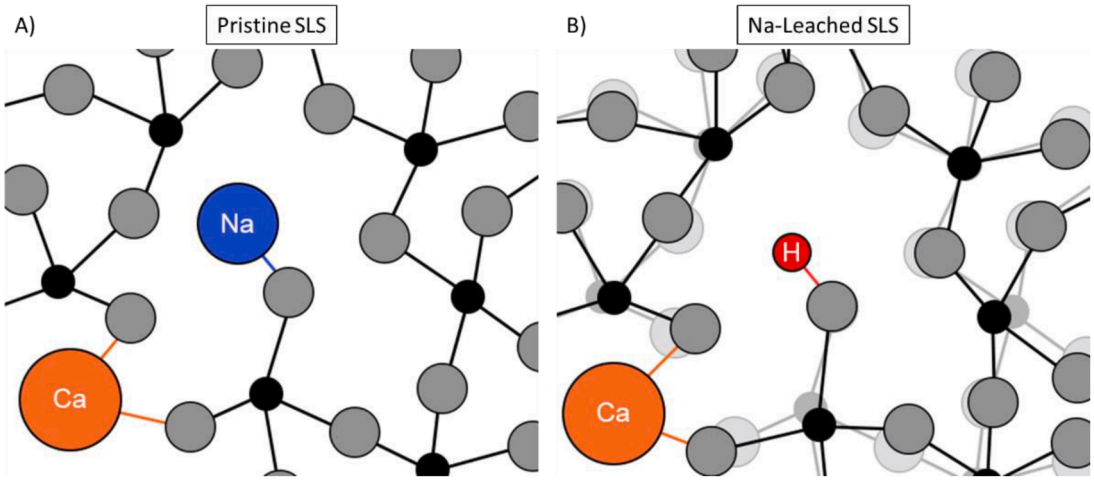

Fig. 5. Two-dimensional projection of the possible localized structural relaxation occurring in SLS after acid treatment around a single sodium. (A) Sodium silicate structure before acid treatment and (B) protonated silica structure after exchange of Na^+ with H^+. The translucent atoms in (B) represent the perturbed location of the BO network before acid treatment, and correspond to the location of the silicate network in (A). Note that this diagram is not drawn to scale.

band and the concentration of NBO species in the glass. [17,42,43] Later, the Si-OH mode was assumed to occur at the same position. [44]

However, this interpretation makes three key oversights. First, the assumption made for spectral interpretation is not correct. The vibrational modes of an isolated SiO_4 tetrahedral or its clusters cannot be identical to the vibrational modes of the same unit when three-dimensionally connected in a silicate glass. Vibrationally active modes can become synchronized due to damping functions associated with connectivity to adjacent units. [45] As these vibrationally active modes are connected within the silicate network, the approach of treating these modes as 'identical' to completely isolated and independent vibrations is not valid, as discussed in our previous publications. [18,46] Changes in vibrational spectra of glass have been directly related to changes in the structure of the vibrationally active modes in the three-dimensionally connected network, [33,34,37] which further proves that the assumption of isolated SiO_4 tetrahedral or its clusters should be discarded.

The second oversight is the use of Beer-Lambert law to deconvolute trends observed in IR spectra collected in the specular reflectance mode. The key term in the Beer-Lambert law is absorbance (A). While absorbance (which is defined as $-\log(T)$, where T is the transmittance) is dimensionally equivalent to the logarithmic change in reflectance ($-\log(R)$, where R is the reflectance measured in SR-IR analysis), they are fundamentally different experimental parameters. This difference is clear from a mathematical perspective, as T is only a function of the imaginary component of the refractive index, while R is a function of both the real and imaginary components. [47] The differences between T and R are discussed in more detail in our previous publication. [16] In other words, the Beer-Lambert law does not hold for vibrational spectrum collected in specular reflection mode, as reflectance could be altered for reasons other than a change in the concentration of the vibrationally active mode. Also note that most SR-IR spectra are plotted in the scale of percent reflectance (or from 0 to 1), not $-\log(R)$.

Finally, if the intensity of the shoulder at 950 cm^{-1} was linearly related to the concentration of NBO species, it would be similar for any binary silicate glasses with the same concentration of equivalent network modifier (NWM) ions. Fig. 6 compares three spectra of alkali silicates with similar concentrations of monovalent alkali ions (Li, Na, and K) from the original work by Sanders et al. [17] When the spectra are no longer normalized, the data clearly shows that the identity of the NWM has a pronounced effect on the intensity of the shoulder at 950 cm^{-1}

In the homologue series of alkali silicates shown in Fig. 6, it is noted that the ratio between the max intensity of the main 1050-1100 cm^{-1} band and the 950 cm^{-1} shoulder appears to correlate with the atomic

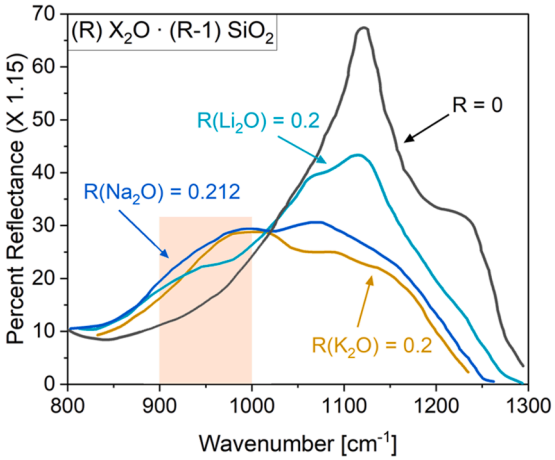

Fig. 6. Vibrational spectra for a series of binary alkali silicate glasses and fused silica replotted from reference [17]. Notice that the sodium silicate, lithium silicate, and potassium silicate all have NWM concentrations close to 20%, yet have very different intensities at 950 cm^{-1}.

radius of the alkali ion (i.e. $r_{Li} < r_{Na} < r_K$). [48] This trend can be well explained if the 950 cm^{-1} band is related to perturbations in the BO network from the NWMs which charge compensate the NBOs in the glass. In the context of this new peak assignment, the larger NWM ions cause the perturbations in the BO network to be more severe, which induces a larger relative increase of the 950 cm^{-1} band and a corresponding decrease of the intensity of the main 1050-1100 cm^{-1} band. This assignment is also consistent with the observations which lead to the original peak assignment, because the degree of BO network perturbations from NWMs will correlate with the NBO concentration.

This new assignment also explains the decrease in intensity of the 950 cm^{-1} shoulder of SLS after acid treatment (Fig. 2). As hydrogen has the smallest ionic radius of any of the modifiers considered, the BO network perturbation would be the least pronounced at the same concentration of NBOs. This decreased perturbation is then manifested as a corresponding decrease at 950 cm^{-1} and a narrowing of the Si-O stretch peak width. This is consistent with the localized structural relaxation shown graphically in Fig. 5. The revised peak assignment is also consistent with the vitreous silica spectra. It has no perturbations in the BO network from NWMs (as $c_{NWM} = 0$), and as a result the 950 cm^{-1} shoulder is negligible (shown in Figs. 2, 4, and 6).

4. Conclusion

Information from vibrational spectroscopy, optical theory, and MD simulations were integrated to elucidate the structure of the Na-leached surface layer on acid-treated SLS. After deconvoluting the interfacial interference in SR-IR which had convoluted previous analysis, nano-FTIR spectra were utilized to observe the spectral changes after Na-H ion-exchange. In the process of deconvoluting the structure of the Na-leached SLS, the traditional peak assignment between the 950 cm^{-1} spectral feature and the concentration of NBOs is found to be physically unrealistic. This spectral feature is instead related to the degree of perturbation of the silicate network from the NWMs which charge compensate the NBOs in the glass. The decreased spectral intensity at 950 cm^{-1} after acid treatment can then be related to localized structural relaxations which result from replacing sodium with hydrogen ions. When leached of sodium, the SLS glass structure had a decreased average Si—BO bond length, an increased average Si—O—Si bond angle, and a narrower O—Si—O bond angle FWHM, all of which correspond to the glass network becoming more 'silica-like'. But it should be noted that this silica-like structure is still distinct from the silica glass structures which result from quenching from the silica melt.

CRediT authorship contribution statement

Andrew L. Ogrinc: Conceptualization, Methodology, Formal analysis, Investigation, Data curation, Writing – original draft, Writing – review & editing, Visualization. **Yuxing Zhou:** Methodology, Software, Investigation, Writing – review & editing. **Seung Ho Hahn:** Software, Investigation, Writing – review & editing. **Yen-Ting Lin:** Software, Validation. **Seong H. Kim:** Conceptualization, Methodology, Writing – review & editing, Supervision, Project administration, Funding acquisition.

Declaration of Competing Interest

The authors declare that they have no known competing financial interests or personal relationships that could have appeared to influence the work reported in this paper

Data Availability

A file with the sSNOM data and the calculations described in the manuscript has been made available online.

Acknowledgments

This work was supported by the National Science Foundation (Grant No. DMR-2011410). The authors acknowledge Dr. Tobias Gokus (attocube Systems/neaspec, Germany) for collection of s-SNOM spectra and assistance with understanding s-SNOM instrumentation, Dr. Shin-Ichi Amma (AGC, Japan) for providing SLS samples and glass compositions, Jeff Shallenberger (Materials Characterization Lab, Penn State) for assistance with troubleshooting during operation of XPS, Dr. Robert Hengstebeck (Materials Characterization Lab, Penn State) for assistance with analysis of the sodium depth profile, Dr. Tawanda Zimudzi (Materials Characterization Lab, Penn State) for assistance with analysis of SR-IR data, and Dr. Maxwell Wetherington (Materials Characterization Lab, Penn State) for collection of Raman spectra.

Supplementary materials

Supplementary material associated with this article can be found, in the online version, at doi:10.1016/j.jnoncrysol.2022.121989.

References

[1] S. Gin, J.M. Delaye, F. Angeli, S. Schuller, Aqueous alteration of silicate glass: state of knowledge and perspectives, npj Mater. Degrad. 5 (2021), https://doi.org/10.1038/s41529-021-00190-5.
[2] N. Sheth, C. Greenley, R. Bermejo, J.C. Mauro, C.G. Pantano, S.H. Kim, Effects of acid leaching treatment of soda lime silicate glass on crack initiation and fracture, J. Am. Ceram. Soc. (2021), https://doi.org/10.1111/jace.17840.
[3] J. Luo, W. Grisales, M. Rabii, C.G. Pantano, S.H. Kim, Differences in surface failure modes of soda lime silica glass under normal indentation versus tangential shear: A comparative study on Na+/K+-ion exchange effects, J. Am. Ceram. Soc. 102 (2019) 1665–1676, https://doi.org/10.1111/jace.16019.
[4] N. Sheth, J. Luo, J. Banerjee, C.G. Pantano, S.H. Kim, Characterization of surface structures of dealkalized soda lime silica glass using X-ray photoelectron, specular reflection infrared, attenuated total reflection infrared and sum frequency generation spectroscopies, J. NonCryst. Solids 474 (2017) 24–31, https://doi.org/10.1016/j.jnoncrysol.2017.08.009.
[5] N. Sheth, S.H. Hahn, D. Ngo, A. Howzen, R. Bermejo, A.C.T. van Duin, J.C. Mauro, C.G. Pantano, S.H. Kim, Influence of acid leaching surface treatment on indentation cracking of soda lime silicate glass, J. NonCryst. Solids 543 (2020), https://doi.org/10.1016/j.jnoncrysol.2020.120144.
[6] D. Strachan, Glass dissolution as a function of pH and its implications for understanding mechanisms and future experiments, Geochim. Cosmochim. Acta 219 (2017) 111–123, https://doi.org/10.1016/j.gca.2017.09.008.
[7] F. Geotti-Bianchini, L. Deriu, G. Gagliardi, M. Guglielmi, C.G. Pantano, New interpretation of the Ir reflectance spectra of Sio2-rich films on soda-lime glass, Glastech. Ber.-Glass. 64 (1991) 205–217.
[8] S.H. Hahn, A.C.T. van Duin, Surface reactivity and leaching of a sodium silicate glass under an aqueous environment: A ReaxFF molecular dynamics study, J. Phys. Chem. C 123 (2019) 15606–15617, https://doi.org/10.1021/acs.jpcc.9b02940.
[9] R.H. Doremus, Interdiffusion of hydrogen and alkali ions in a glass surface, J. NonCryst. Solids 19 (1975) 137–144, https://doi.org/10.1016/0022-3093(75)90079-4.
[10] N. Sheth, D. Ngo, J. Banerjee, Y. Zhou, C.G. Pantano, S.H. Kim, Probing hydrogen-bonding interactions of water molecules adsorbed on silica, sodium calcium silicate, and calcium aluminosilicate glasses, J. Phys. Chem. C 122 (2018) 17792–17801, https://doi.org/10.1021/acs.jpcc.8b04233.
[11] S.i. Amma, J. Luo, S.H. Kim, C.G. Pantano, Effect of glass composition on the hardness of surface layers on aluminosilicate glasses formed through reaction with strong acid, J. Am. Ceram. Soc. 101 (2017) 657–665, https://doi.org/10.1111/jace.15239.
[12] S. Amma, J.W. Luo, S.H. Kim, C.G. Pantano, Effects of fictive temperature on the leaching of soda lime silica glass surfaces, J. Am. Ceram. Soc. 100 (2017) 1424–1431, https://doi.org/10.1111/jace.14754.
[13] B.P. McGrail, L.R. Pederson, D.A. Petersen, The influence of surface potential and pH on the release of sodium from Na2O.3SiO2 glass, Phys. Chem. Glasses 27 (1986) 59–64.
[14] I. Carazeanu Popovici, N. Lupascu, Chemical durability of soda-lime glass in aqueous acid solutions, Analele Universitatii "Ovidius", Constanta - Seria Chimie 23 (2012) 128–132, https://doi.org/10.2478/v10310-012-0021-6.
[15] D.E. Clark, M.F. Dilmore, E.C. Ethridge, L.L. Hench, Aqueous corrosion of soda-silica and soda-lime-silica glass, J. Am. Ceram. Soc. 59 (1976) 62–65, https://doi.org/10.1111/j.1151-2916.1976.tb09391.x.
[16] S.-i. Amma, J. Luo, C.G. Pantano, S.H. Kim, Specular reflectance (SR) and attenuated total reflectance (ATR) infrared (IR) spectroscopy of transparent flat glass surfaces: a case study for soda lime float glass, J. NonCryst. Solids 428 (2015) 189–196, https://doi.org/10.1016/j.jnoncrysol.2015.08.015.
[17] D.M. Sanders, W.B. Person, L.L. Hench, Quantitative analysis of glass structure with the use of infrared reflection spectra, Appl. Spectrosc. 28 (1974) 247–255, https://doi.org/10.1366/000370274774332623.
[18] J. Luo, N.J. Smith, C.G. Pantano, S.H. Kim, Complex refractive index of silica, silicate, borosilicate, and boroaluminosilicate glasses – Analysis of glass network vibration modes with specular-reflection IR spectroscopy, J. NonCryst. Solids 494 (2018) 94–103, https://doi.org/10.1016/j.jnoncrysol.2018.04.050.
[19] H. Kaya, D. Ngo, N.J. Smith, S. Gin, S.H. Kim, Network structure in alteration layer of boroaluminosilicate glass formed by aqueous corrosion, J. NonCryst. Solids 553 (2021), https://doi.org/10.1016/j.jnoncrysol.2020.120494.
[20] H. Fujiwara, Spectroscopic Ellipsometry: Principles and Applications, 2007.
[21] H.T. He, Z. Chen, Y.T. Lin, S.H. Hahn, J.X. Yu, A.C.T. van Duin, T.D. Gokus, S. V. Rotkin, S.H. Kim, Subsurface structural change of silica upon nanoscale physical contact: chemical plasticity beyond topographic elasticity, Acta Mater. 208 (2021), 116694, https://doi.org/10.1016/j.actamat.2021.116694.
[22] L. Mester, A.A. Govyadinov, S. Chen, M. Goikoetxea, R. Hillenbrand, Subsurface chemical nanoidentification by nano-FTIR spectroscopy, Nat. Commun. 11 (2020) 3359, https://doi.org/10.1038/s41467-020-17034-6.
[23] L. Mester, A.A. Govyadinov, R. Hillenbrand, High-fidelity nano-FTIR spectroscopy by on-pixel normalization of signal harmonics, Nanophotonics 11 (2021) 377–390, https://doi.org/10.1515/nanoph-2021-0565.
[24] G.H. Frischat, Tin ions in float glass cause anomalies, Cr Chim. 5 (2002) 759–763, https://doi.org/10.1016/S1631-0748(02)01436-4.
[25] M.H. Krohn, J.R. Hellmann, B. Mahieu, C.G. Pantano, Effect of tin-oxide on the physical properties of soda-lime–silica glass, J. NonCryst. Solids 351 (2005) 455–465, https://doi.org/10.1016/j.jnoncrysol.2005.01.050.
[26] J. Banerjee, S.H. Kim, C.G. Pantano, Elemental areal density calculation and oxygen speciation for flat glass surfaces using x-ray photoelectron spectroscopy,

J. NonCryst. Solids 450 (2016) 185–193, https://doi.org/10.1016/j.jnoncrysol.2016.07.029.
[27] J.C. Vickerman, I.S. Gilmore, Surface Analysis– The Principal Techniques, 2009.
[28] K. Satori, Y. Haga, R. Minatoya, M. Aoki, K. Kajiwara, Factors causing deterioration of depth resolution in Auger electron spectroscopy depth profiling of multilayered systems, J. Vac. Sci. Technol. A 15 (1997) 478–484, https://doi.org/10.1116/1.580877.
[29] S. Hofmann, Sputter depth profiling of thin films, High Temp. Mat. Pr-Isr 17 (1998) 13–27.
[30] S. Bruns, T. Uesbeck, S. Fuhrmann, M.T. Aymerich, L. Wondraczek, D. de Ligny, K. Durst, Indentation densification of fused silica assessed by raman spectroscopy and constitutive finite element analysis, J. Am. Ceram. Soc. 103 (2020) 3076–3088, https://doi.org/10.1111/jace.17024.
[31] D.R. Neuville, D. de Ligny, G.S. Henderson, Advances in Raman spectroscopy applied to earth and material sciences, Rev. Mineral. Geochem. 78 (2014) 509–541, https://doi.org/10.2138/rmg.2013.78.13.
[32] L. Deng, S. Urata, Y. Takimoto, T. Miyajima, S.H. Hahn, A.C.T. Duin, J. Du, Structural features of sodium silicate glasses from reactive force field-based molecular dynamics simulations, J. Am. Ceram. Soc. 103 (2019) 1600–1614, https://doi.org/10.1111/jace.16837.
[33] H.S. Liu, S.H. Hahn, M.G. Ren, M. Thiruvillamalai, T.M. Gross, J.C. Du, A.C.T. van Duin, S.H. Kim, Searching for correlations between vibrational spectral features and structural parameters of silicate glass network, J. Am. Ceram. Soc. 103 (2020) 3575–3589, https://doi.org/10.1111/jace.17036.
[34] J. Luo, Y. Zhou, C.G. Pantano, S.H. Kim, Correlation between IR peak position and bond parameter of silica glass: Molecular dynamics study on fictive temperature (cooling rate) effect, J. Am. Ceram. Soc. 101 (2018) 5419–5427, https://doi.org/10.1111/jace.15858.
[35] A.C.T. van Duin, S. Dasgupta, F. Lorant, W.A. Goddard, ReaxFF: A reactive force field for hydrocarbons, J. Phys. Chem. A 105 (2001) 9396–9409, https://doi.org/10.1021/jp004368u.
[36] S.H. Hahn, J. Rimsza, L. Criscenti, W. Sun, L. Deng, J.C. Du, T. Liang, S.B. Sinnott, A.C.T. van Duin, Development of a ReaxFF reactive force field for NaSiOx/Water systems and its application to sodium and proton self-diffusion, J. Phys. Chem. 122 (2018) 19613–19624, https://doi.org/10.1021/acs.jpcc.8b05852.
[37] J. Luo, Y. Zhou, S.T. Milner, C.G. Pantano, S.H. Kim, Molecular dynamics study of correlations between IR peak position and bond parameters of silica and silicate glasses: effects of temperature and stress, J. Am. Ceram. Soc. 101 (2017) 178–188, https://doi.org/10.1111/jace.15187.
[38] J. Banerjee, V. Bojan, C.G. Pantano, S.H. Kim, Effect of heat treatment on the surface chemical structure of glass: oxygen speciation from in situ XPS analysis, J. Am. Ceram. Soc. 101 (2017) 644–656, https://doi.org/10.1111/jace.15245.
[39] C. Calahoo, J.W. Zwanziger, I.S. Butler, Mechanical–structural investigation of ion-exchanged lithium silicate glass using micro-raman spectroscopy, J. Phys. Chem. C 120 (2016) 7213–7232, https://doi.org/10.1021/acs.jpcc.6b01720.
[40] J.W. Luo, H. Huynh, C.G. Pantano, S.H. Kim, Hydrothermal reactions of soda lime silica glass - Revealing subsurface damage and alteration of mechanical properties and chemical structure of glass surfaces, J. NonCryst. Solids 452 (2016) 93–101, https://doi.org/10.1016/j.jnoncrysol.2016.08.021.
[41] J. Luo, H. He, N.J. Podraza, L. Qian, C.G. Pantano, S.H. Kim, J. Mauro, Thermal poling of soda-lime silica glass with nonblocking electrodes-part 1: effects of sodium ion migration and water ingress on glass surface structure, J. Am. Ceram. Soc. 99 (2016) 1221–1230, https://doi.org/10.1111/jace.14081.
[42] F. Gervais, A. Blin, D. Massiot, J.P. Coutures, M.H. Chopinet, F. Naudin, Infrared reflectivity spectroscopy of silicate-glasses, J. NonCryst. Solids 89 (1987) 384–401, https://doi.org/10.1016/S0022-3093(87)80280-6.
[43] C.A. Murray, T.J. Greytak, Intrinsic surface phonons in amorphous silica, Phys. Rev. B 20 (1979) 3368–3387, https://doi.org/10.1103/PhysRevB.20.3368.
[44] F. Orgaz, H. Rawson, Colored coatings prepared by the sol-gel process, J. NonCryst. Solids 82 (1986) 378–390, https://doi.org/10.1016/0022-3093(86)90155-9.
[45] B. Chen, X. Xia, X. Wang, Synchronization and vibratory synchronization transmission of a weakly damped far-resonance vibrating system, PLoS One 14 (2019), e0209703, https://doi.org/10.1371/journal.pone.0209703.
[46] H.S. Liu, H. Kaya, Y.T. Lin, A. Ogrinc, S.H. Kim, Vibrational spectroscopy analysis of silica and silicate glass networks, J. Am. Ceram. Soc. 105 (2022) 2355–2384, https://doi.org/10.1111/jace.18206.
[47] M. Rubin, Optical properties of soda lime silica glasses, Sol. Energy Mater. 12 (1985) 275–288, https://doi.org/10.1016/0165-1633(85)90052-8.
[48] R.D. Shannon, Revised effective ionic radii and systematic studies of interatomic distances in halides and chalcogenides, Acta Crystallogr., Sect. A 32 (1976) 751–767, https://doi.org/10.1107/s0567739476001551.